Article:

Gao, J, Chen, H, Chen, J et al. (3 more authors) (2019) Explorations on the continuous oxidation kinetics of diesel PM from heavy-duty vehicles using a single ramp rate method. Fuel, 248. pp. 254-257. ISSN 0016-2361

https://doi.org/10.1016/j.fuel.2019.02.127

Explorations on the continuous oxidation kinetics of diesel PM using single ramp rate method

Jianbing Gao[a,b], Haibo Chen[b,*], Junyan Chen[b], Chaochen Ma[a,*], Guohong Tian[c], Ying Li[d]

a. School of Mechanical Engineering, Beijing Institute of Technology, Beijing 100081, China
b. Institute for Transport Studies, University of Leeds, Leeds LS2 9JT, UK
c. Department of Mechanical Engineering Sciences, University of Surrey, Guildford GU2 7XH, UK
d. WOCH Ltd, Castleford WF10 5TH, UK

[*] Corresponding author:
Chaochen Ma
E-mail:machaochen1900@163.com
Haibo Chen
E-mail: H.Chen@its.leeds.ac.uk

Abstract

Particulate matter (PM) emitted by internal combustion engines has brought about serious environmental problems. Investigations of the PM oxidation behaviors and kinetics make the foundations of decreasing PM emission and working out the regeneration problems of PM capture devices. In this paper, the oxidation kinetics and microstructure evolutions of diesel PM in the oxidation process were researched. The results showed that thermogravimetric analysis (TGA) temperature history had a limited influence on the tendency of the oxidation kinetics. The volatilization of the organic compounds dominated the mass loss without any heat release at the initial stage of PM oxidation. The abnormal phenomenon (negative apparent activation energy) was observed in the oxidation process when the oxidation temperature was in the range of 200°C~ 340°C, which was ubiquitous during PM oxidation. However, the abnormal phenomenon disappeared if the PM sample was pre-treated to remove the volatile organic compounds (VOC), with the result that the phenomenon was caused by the VOC. The hydrogen bonding complex was formed in that temperature range, where the energy of the hydrogen bonding complex was lower than the value of the reactants, which caused the negative apparent activation energy. The apparent activation energy increased gradually when the temperature was higher than 340°C.

Keywords: diesel particulate matter; oxidation kinetics; microstructure evolutions; negative activation energy

1. Introduction

Large amounts of diesel particles were emitted into the atmosphere, which had a huge potential impact on the environment. Ammann's results [1] showed that the heterogeneous production of HNO_2 from NO_2 suspending on soot particles was 10^5~10^7 times faster than previously reported surface suspending reactions, which implied that soot particles also promoted the formation of photochemical smog. Michelsen et. al [2] reviewed the soot formation, evolutions and oxidation, with the results that the active radicals (such as OH, O, CH and CH_2) played a vital role at the initial stage of soot formation process. Meantime, the soot agglomerates and graphitic aggregates happened, which restuled in the stable soot particles. Deeply investigating the PM oxidation behaviors and oxidation kinetics contributed to decreasing the PM emission and to optimizing the PM removal devices, such as diesel particulate filters (DPFs) [3] and non-thermal plasma (NTP) reactors [4].

PM nanostructures of a light-duty diesel engine [5], the effect of exhaust gas recirculation (EGR) on PM oxidation activity [6], diesel PM oxidation behaviors [7, 8], and PM oxidation model [9] were widely investigated. Vander Wal et.al [10] quantified the soot nanostructures using fringe separation distance, fringe length and tortuosity, which revealed the relations of the soot nanostructures and PM formation temperature. Further, the influence of the heat-treatment temperature on the soot nanostructures was investigated that the crystallites were more orderly arranged after heat-treatment [11]. The statistics of the primary particle diameters were made based on the soot morphology, which showed closely related to oxidation activity [12], that the average value was between 20 nm and 25 nm. Qu et. al [13] investigated the oxidation activity of biodiesel PM, which presented closely related to the oxygen and VOC contents of biodiesel PM. López-Fonseca et. al [14] calculated the oxidation kinetics using different reaction models, with the conclusions that the choose of the reaction models significantly influenced the oxidation activity. The commonly used methods to calculate the PM oxidation kinetics were based on single ramp rate and multi-ramp rate thermogravimetric analysis (TGA) profiles using Arrhenius equation [4, 15, 16]. Multi-ramp rate method in this paper was that at least three TGA profiles obtained at different ramp rates were needed to calculate the oxidation kinetics. Sharma et. al [15] investigated the oxidation kinetics using single ramp rate method that the activation energy was almost the same in a small temperature range. The samples used for the TGA experiments were raw PM or pre-treated PM at high temperature, non-oxidizing atmosphere. As for the raw PM, the oxidation and volatilization happened simultaneously for volatile organic compounds (VOC) contained in the diesel PM, which led to the distortions of the oxidation kinetic lines. The oxidation kinetic lines were missed at the low temperature regions if PM samples were pre-treated at high temperature atmosphere to remove the VOC; also, high temperature pre-treatment significantly decreased the oxidation activity. The differential scanning calorimetry (DSC) device detected the heat release rate as the function of oxidation temperature [4]. This method effectively detected the PM oxidation temperature and oxidation intensity at low temperature regions based on the heat loss during oxidation. The single ramp rate method presented the oxidation kinetic changes continuously in the oxidation process. The oxidation kinetic calculations using DSC profiles based on the single ramp rate method was seldomly reported to the authors' knowledge. As can be seen from the references [17, 18], the details of the oxidation kinetics based on multi-ramp rate method were neglected due to the large temperature intervals. The oxidation kinetics based on the single ramp rate method in references [19, 20] were only focused on the high temperature zones.

In this paper, the TGA and DSC profiles were combined to investigate the PM oxidation kinetics in the whole oxidation process. The single ramp rate method was used to research the details of the oxidation kinetics. The sketches of microstructure evolutions in PM oxidation process were assisted to clarify PM oxidation kinetics. With emphasis, the non-reported abnormal phenomenon of diesel PM oxidation kinetics in the oxidation process was discovered and analyzed.

2. Oxidation kinetics lines extraction

Calculations of the oxidation kinetics using oxidation profiles is based on Arrhenius equation (Equation 1) and its transformation is as Equation 2,

$$k=A\exp(-\frac{E}{RT}) \qquad (1)$$

$$-\frac{\mathrm{d}m}{\mathrm{d}t}=km^{n}p_{\mathrm{O}_2}^{r}=A\exp(-\frac{E}{RT})m^{n}p_{\mathrm{O}_2}^{r} \qquad (2)$$

Where m, t, k, n, p_{O2}, r, A, E, R, T are sample mass, time, reaction rate constant, reaction order for carbon, partial pressure of oxygen, reaction order for oxygen, pre-exponential factor, apparent activation energy, universal gas constant (8.314 J/mol·K) and temperature. References [15, 21] showed that the reaction orders of different soot were close to unit (1.0). So that Equation 2 is transferred into Equation 3,

$$\ln\left(-\frac{\mathrm{d}m}{m\cdot\mathrm{d}t}\right)=\ln\left(\mathrm{A}p_{\mathrm{O}_2}\right)-\frac{E}{RT} \qquad (3)$$

In the oxidation process of a narrow temperature range, ln(-dm/(m·dt)) shows a linear correlation with -/(R·T). E and A could be calculated from the slope and intercept of Equation 3. In the oxidation process, the slope and intercept changed gradually, resulting from the changes of the physicochemical properties, including ingredients (such soot, SOF and salts), structures, oxygen contents [4, 22].

3. TGA and DSC profiles

In order to decrease the experimental errors, vacant combustion in air was performed to remove the residuals before TGA and DSC experiments. The duplicate tests of TGA experiments are shown in Figure. S1. As can be seen, the repeatability of the experiments is excellent. The calculations of oxidation kinetic lines were based on TGA and DSC profiles. The oxidation profiles based on TGA and DSC experiments are shown in Figure 1, and parts of these curves were reported in reference [4]. Diesel PM samples A and B were collected at 60% and 80% engine load conditions, respectively. Devolatilized sample A was obtained by pre-treating sample A at high temperature, non-oxidizing atmosphere, the pre-treatment process was as the following: sample A was heated from room temperature to 450 °C at a 20 °C/min ramp rate in N_2 atmosphere and was kept at 450 °C isothermal condition for 15 minutes; Then, it was cooled to atmosphere temperature. The DSC profiles were obtained by the normalization of the heat release curves, in which the assumption was made that the heat release rate was proportional to the PM mass loss rate caused by oxidation (rather than the volatilization). The detailed discussions about the TGA and DSC profiles were presented in reference [4]. Reference [13] indicated that oxidation and volatilization happened simultaneously when the temperature was lower than 350 °C, which was similar to the authors' research. Also, reference [19] defined the mass loss caused by low volatility and high volatility which were in the ranges of 200 °C~500 °C and 40 °C~200 °C, respectively. Advanced technologies should be adopted to further clearly distinguish the oxidation and volatilization. This paper was mainly focused on the details of the oxidation kinetics during PM oxidation.

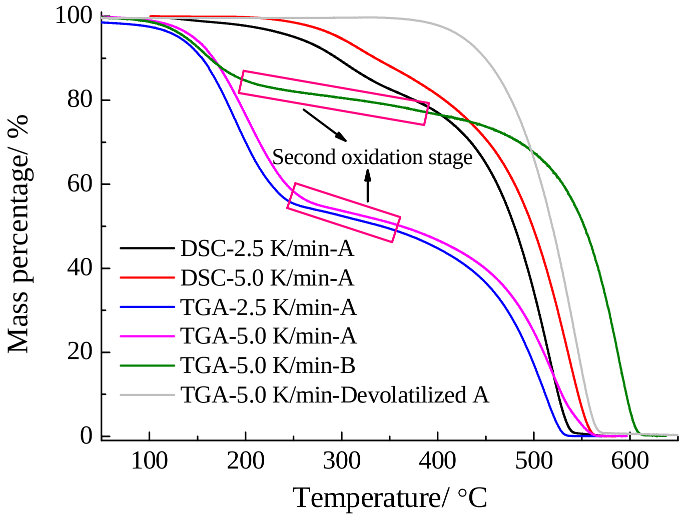

Figure 1 Diesel PM oxidation profiles based on TGA and DSC experiments [4]

4. Oxidation kinetics analysis

Details of the oxidation kinetics in the oxidation process were neglected if the multi-ramp rate method was used due to the temperature intervals, as showed in references [4, 18]. However, the oxidation kinetics based on the single ramp rate method was continuous, which could clearly indicate the details in the whole oxidation process. Figure 2 shows the oxidation kinetic lines and microstructure evolutions in the oxidation process. Based on the microstructure evolutions, the phenomenons in the oxidation process could be more clearly clarified. The slopes of the oxidation kinetic lines reflected the apparent activation energy [23]. The tendency of the apparent activation energy in the oxidation process was similar at different ramp rate conditions for DSC based method, as shown in Figure 2(b). Similarly, the ramp rates had a small influence on the tendency of apparent activation energy for TGA based method (Figure 2(a)). Apparent activation energy was almost the same when the oxidation temperature was lower than 310 °C;

then, it dropped to below zero around 344 °C and increased gradually in the following oxidation process for the DSC based method. Compared with the TGA based oxidation kinetic lines, the DSC based kinetic lines were smoother due to the fact that the DSC device tested the heat release free of the vibration and noise effects. The differences of the apparent activation energy tendency for the TGA and DSC methods were mainly focused on the low temperature regions, where the temperature was lower than 344 °C (it was exampled using sample A at 5.0 °C/min ramp rate). The apparent activation energy changed little when the temperature was lower than 200 °C, where the volitalization dominated the mass loss; then, it decreased in the temperature ranges of 200 °C~344 °C. The tendency was the same by comparing samples A and B, while the differences were mainly focused on the characteristic temperatures, such as the temperature where the transitions of the apparent activation energy happened. For the pre-treated PM sample (devolatilized A), the apparent activation energy was almost the same in the temperature range of 340 °C~530 °C, where the oxidation dominated the reactions; it increased rapidly after that temperature range. It seemed that the pre-treatment at non-oxidizing atmosphere had a small effect on the apparent activation energy at high temperature zones. Reference [15] calculated the diesel soot oxidation kinetics using single ramp rate method that the apparent activation energy was almost kept at the same value in the temperature range of 515 °C~635 °C. The phenomenon was similar to the devolatilized PM in this paper. Wang et. al [19] indicated that the changes of the apparent activation energy in the oxidation process using single ramp rate method were much smaller for low ramp rate than that of high ramp rate in the temperature range of 410 °C~525 °C.

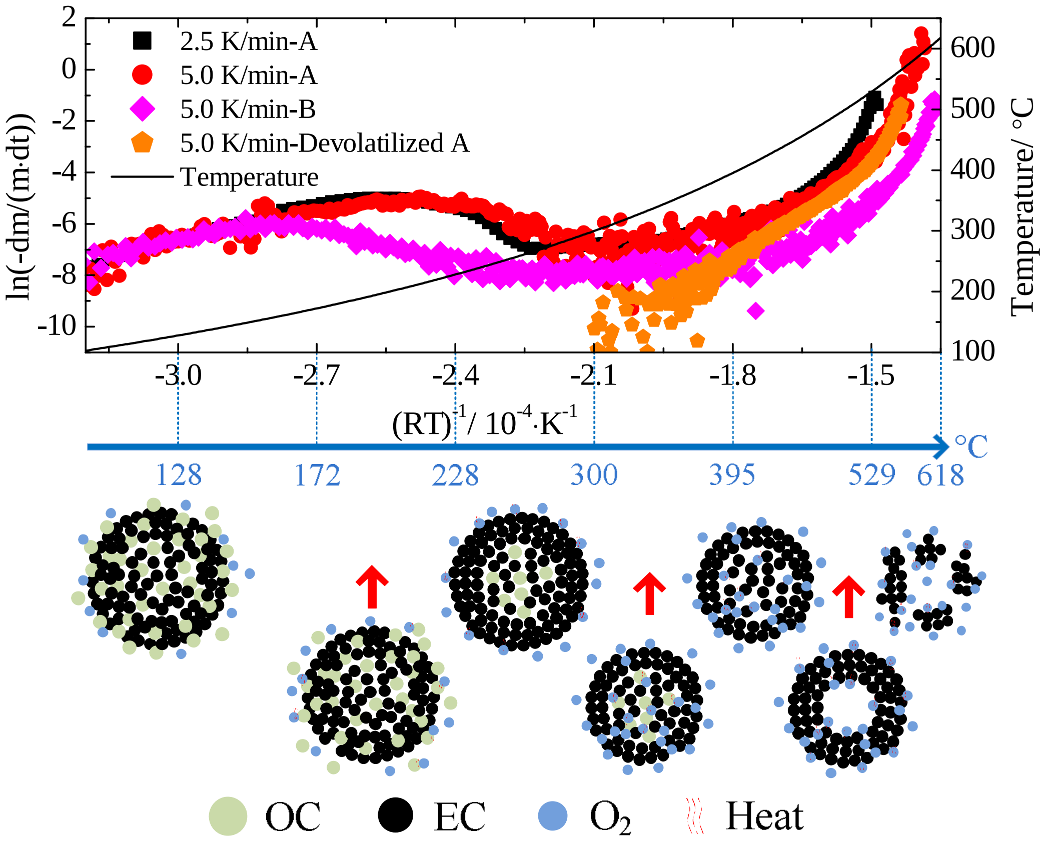

(a) Oxidation kinetic lines based on TGA profiles and microstructure evolutions

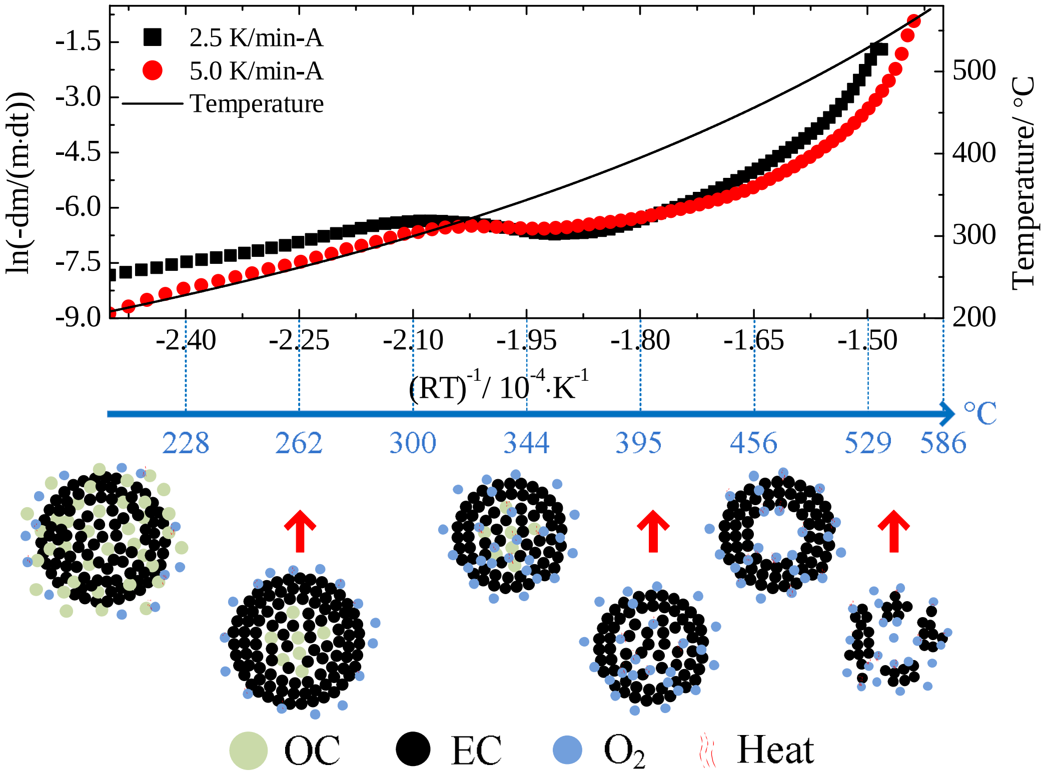

(b) Oxidation kinetic lines based on DSC profiles and microstructure evolutions

Figure 2 Oxidation kinetic lines and microstructure evolutions: OC, organic carbon; EC, element carbon

Sample A (5.0 K/min ramp rate) was taken as the example to detailed illustrate the oxidation kinetic phenomenon in the oxidation process. For the TGA based method, the apparent activation energy was nearly a constant value when the temperature was lower than 200 °C, however, the volatilization dominated the reaction at the temperature region as indicated in DSC profiles (Figure 1). This phenomenon was similar to the results in the reference [24]. Actually, the apparent activation energy in the region was the energy that was needed to volatilize the low molecular VOC contained in the diesel PM. As shown in the microstructure evolutions in Figure 2(a), only the surface VOC volatilization happened at this stage. Chemical reactions happened for VOC when the temperature was higher than 200 °C. While the chemical reactions dominated mass loss when temperature was higher than 250 °C, which could be gotten by comparing the TGA and DSC based oxidation profiles. In the temperature zone, chemical reactions and volatilization happened simultaneously with heat release. Soot surfaces were oxidized gradually with the following results that the oxidation was transferred from the surfaces to inner cores at high temperature conditions.

In the temperature range of 200 °C~310 °C, an abnormal phenomenon was observed that the apparent activation energy calculated using TGA based profiles was the negative, however, it was positive for DSC based profiles. During the temperature region, the mass loss percentage for the TGA methods was high, however, the heat release was low. Pyrolysis reactions happened in this process, where the high molecular VOC was broken up into low molecular VOC, whose volatilization temperature was low. The pyrolysis reactions of high molecular VOC led to the rapidly decrease of PM mass. The pyrolysis reactions caused the negative apparent activation energy in TGA based method, and the detailed reasons would be discussed below. Much high molecular VOC was converted into low molecular VOC that most of the low molecular VOC flowed out of the TGA device. Due to the high atmosphere temperature in TGA device, part of low molecular VOC was oxidized once the high molecular VOC was broken up, which caused the heat release during this stage. So that the TGA based kinetic lines partly depicted the pyrolysis reactions of high molecular VOC during this temperature region, while it was low molecular VOC oxidation in DSC based kinetic lines.

In the small temperature range of 310 °C~ 340 °C, the apparent activation energy was negative or around zero for both the TGA and DSC based methods. The mass loss rate was low in this temperature region. The abnormal phenomenon was ubiquitous during the PM oxidation, it can be known by comparing the oxidation kinetic lines of samples A and B. However, the phenomenon was neglected in all the reported researches about PM oxidation kinetics to the authors' knowledge [25-27]. This was mainly caused by the multi-ramp rate method calculating the oxidation kinetics, and PM pre-treatment at high temperature conditions. For different PM samples, the discrepancy was mainly focused on the positions and durations of the abnormal phenomenon, as presented in Figure 2(a). Also, it seemed that the durations of the abnormal phenomenon showed closely related to the high molecular VOC content and the second oxidation phase (slow oxidation in Figure 1), which was concluded by correlating Figure 1. The low molecular VOC content was almost the same for samples A and B (mass loss when temperature was lower than 200 °C). Evidently, the second oxidation phase lasted a wide temperature region, which resulted of the huge temperature range of the abnormal phenomenon. The abnormal phenomenon disappeared when the sample was pre-treated at high temperature atmosphere to remove the VOC (devolatilized sample A). So that it was concluded by comparing sample A and devolatilized sample A that the abnormal phenomenon was caused by VOC. Smith et. al [28] summarized large amounts of elementary reactions, with the conclusion that the apparent activation energy was negative for the elementary reaction in a narrow temperature range. Also, the abnormal phenomenon in chemical reactions was reported in other chemical reaction process [29-31].

The general chemical reactions had the positive temperature effect that the reaction rate constant increased with temperature. The apparent activation energy was smaller than zero if the chemical reactions were the negative temperature effect. The negative temperature effect happened in the abnormal periods. It was considered that the hydrogen bonding complex was formed during the oxidation that the energy of the hydrogen bonding complex was lower than the value of the reactants, which led to the negative apparent activation energy [28]. Much hydrogen bonding complex was formed in the abnormal temperature zone, which was the main reason leading to the low mass loss rate in the following reactions despite the temperature increased continually. The reason caused the abnormal phenomenon was same for the temperature range of 200 °C~310 °C in the TGA based method. After the abnormal period, the apparent activation energy increased gradually with the oxidation reaction proceeding.

5. Conclusions

In order to get the details of the oxidation kinetics in diesel PM oxidation process, the oxidation kinetics based on DSC and TGA profiles using single ramp rate method were researched. Meantime, the microstructure evolutions in the diesel PM oxidation process were assisted to clearly clarify the oxidation kinetics. At the initial stage of PM oxidation, VOC volatilization dominated the mass loss and no chemical reactions happened. Large amounts of high molecular VOC were breakup into low molecular VOC, which caused the abnormal phenomenon, negative apparent activation energy, in the temperature range of 200 °C~310 °C in the TGA based method. Meantime, the oxidation of part low molecular VOC released heat in that temperature range. The abnormal phenomenon was also observed in the temperature range of 310 °C~340 °C, where hydrogen bonding complex, with low energy being smaller than the values of reactants, was formed. In addition, the hydrogen bonding complex caused the slow oxidation activity in the following reaction process. The apparent activation energy increased gradually when the temperature was higher than 340 °C. The abnormal phenomenon was ubiquitous during diesel PM oxidation and it disappeared after being pre-treated at high temperature conditions, which indicated that the abnormal phenomenon was caused by the VOC contained diesel PM.

Acknowledgement

The research described in this paper was supported in part by the EU-funded project optiTruck (grant agreement No 713788) which has the ultimate aim to develop and test a prototype ‘global 490 optimizer’, capable of achieving a fuel reduction of at least 20% for 40 tonne trucks while still meeting relevant Euro VI emission standards.

Reference

[1] Ammann M, Kalberer M, Jost D, Tobler L, Rössler E, Piguet D, et al. Heterogeneous production of nitrous acid on soot in polluted air masses. Nature 1998;395(6698):157.

[2] Michelsen H. Probing soot formation, chemical and physical evolution, and oxidation: A review of in situ diagnostic techniques and needs. Proceedings of the Combustion Institute 2017;36(1):717-35.

[3] Jiao P, Li Z, Shen B, Zhang W, Kong X, Jiang R. Research of DPF regeneration with NOx-PM coupled chemical reaction. Appl Therm Eng 2017;110:737-45.

[4] Gao J, Ma C, Xing S, Sun L. Oxidation behaviours of particulate matter emitted by a diesel engine equipped with a NTP device. Appl Therm Eng 2017;119:593-602.

[5] Vander Wal RL, Strzelec A, Toops TJ, Daw CS, Genzale CLJF. Forensics of soot: C5-related nanostructure as a diagnostic of in-cylinder chemistry. 2013;113:522-6.

[6] Al-Qurashi K, Boehman AL. Impact of exhaust gas recirculation (EGR) on the oxidative reactivity of diesel engine soot. CoFl 2008;155(4):675-95.

[7] Strzelec A, Toops T, Daw C, Foster DE, Rutland C. SAE Technical Paper 2010-01-2127, https://doi.org/10.4271/2010-01-2127, SAE 2010 Powertrains Fuels & Lubricants Meeting.

[8] Jaramillo IC, Gaddam CK, Vander Wal RL, Lighty JS. Effect of nanostructure, oxidative pressure and extent of oxidation on model carbon reactivity. CoFl 2015;162(5):1848-56.

[9] Lee J, Tzanetakis T, Zhang Y, Traver M, Lewis S, Moses-DeBusk M, et al. Characterization of Particulate Matter Emissions from Heavy-Duty Partially Premixed Compression Ignition with Gasoline-Range Fuels. SAE Technical Paper 2019-01-1185, https://doi.org/10.4271/2017-01-0932, WCX: SAE World Congress Experience (in press).

[10] Vander Wal RL, Tomasek AJ, Pamphlet MI, Taylor CD, Thompson WK. Analysis of HRTEM images for carbon nanostructure quantification. JNR 2004;6(6):555-68.

[11] Yehliu K, Vander Wal RL, Boehman AL. A comparison of soot nanostructure obtained using two high resolution transmission electron microscopy image analysis algorithms. Carbon 2011;49(13):4256-68.

[12] Barone TL, Storey JM, Youngquist AD, Szybist JPJAE. An analysis of direct-injection spark-ignition (DISI) soot morphology. 2012;49:268-74.

[13] Qu L, Wang Z, Zhang J. Influence of waste cooking oil biodiesel on oxidation reactivity and nanostructure of particulate matter from diesel engine. Fuel 2016;181:389-95.

[14] López-Fonseca R, Landa I, Elizundia U, Gutiérrez-Ortiz M, González-Velasco J. A kinetic study of the combustion of porous synthetic soot. Chem Eng J 2007;129(1):41-9.

[15] Sharma HN, Pahalagedara L, Joshi A, Suib SL, Mhadeshwar AB. Experimental study of carbon black and diesel engine soot oxidation kinetics using thermogravimetric analysis. Energy Fuels 2012;26(9):5613-25.

[16] Darcy P, Da Costa P, Mellottée H, Trichard J-M, Djega-Mariadassou G. Kinetics of catalyzed and non-catalyzed oxidation of soot from a diesel engine. Catal Today 2007;119(1):252-6.

[17] Meng Z, Yang D, Yan Y. Study of carbon black oxidation behavior under different heating rates. JTAC 2014;118(1):551-9.

[18] Ma C, Gao J, Zhong L, Xing S. Experimental investigation of the oxidation behaviour and thermal kinetics of diesel particulate matter with non-thermal plasma. Appl Therm Eng 2016;99:1110-8.

[19] Wang C, Xu H, Herreros JM, Lattimore T, Shuai S. Fuel effect on particulate matter composition and soot oxidation in a direct-injection spark ignition (DISI) engine. Energy Fuels 2014;28(3):2003-12.

[20] Chong HS, Aggarwal SK, Lee KO, Yang SY, Seong H. Experimental investigation on the oxidation characteristics of diesel particulates relevant to DPF regeneration. CST 2013;185(1):95-121.

[21] Stanmore BR, Brilhac J-F, Gilot P. The oxidation of soot: a review of experiments, mechanisms and models. Carbon 2001;39(15):2247-68.

[22] Gao J, Ma C, Xing S, Sun L, Huang L. A review of fundamental factors affecting diesel PM oxidation behaviors. Science China Technological Sciences 2018;61(3):330–45.

[23] Jung H, Kittelson DB, Zachariah MR. The influence of a cerium additive on ultrafine diesel particle emissions and kinetics of oxidation. CoFl 2005;142(3):276-88.

[24] Wang-Hansen C, Ericsson P, Lundberg B, Skoglundh M, Carlsson P-A, Andersson B. Characterization of particulate matter from direct injected gasoline engines. ToCat 2013;56(1-8):446-51.

[25] Karin P, Boonsakda J, Siricholathum K, Saenkhumvong E, Charoenphonphanich C, Hanamura K. Morphology and oxidation kinetics of CI engine's biodiesel particulate matters on cordierite Diesel Particulate Filters using TGA. International Journal of Automotive Technology 2017;18(1):31-40.

[26] López-Fonseca R, Landa I, Gutiérrez-Ortiz M, González-Velasco J. Non-isothermal analysis of the kinetics of the combustion of carbonaceous materials. JTAC 2005;80(1):65-9.

[27] Alozie NS, Fern G, Peirce D, Ganippa L. Influence of Biodiesel Blending on Particulate Matter (PM) Oxidation Characteristics. SAE Technical Paper 2017-01-0932, https://doi.org/10.4271/2017-01-0932, WCX™ 17: SAE World Congress Experience.

[28] Smith IW, Ravishankara A. Role of hydrogen-bonded intermediates in the bimolecular reactions of the hydroxyl radical. The Journal of Physical Chemistry A 2002;106(19):4798-807.

[29] Valverde JM. On the negative activation energy for limestone calcination at high temperatures nearby equilibrium. ChEnS 2015;132:169-77.

[30] Bhunia A, Bansal K, Henini M, Alshammari MS, Datta S. Negative activation energy and dielectric signatures of excitons and excitonic Mott transitions in quantum confined laser structures. JAP 2016;120(14):144304.

[31] Wang Y, Widmann D, Wittmann M, Lehnert F, Gu D, Schüth F, et al. High activity and negative apparent activation energy in low-temperature CO oxidation–present on Au/Mg (OH) 2, absent on Au/TiO 2. Catalysis Science & Technology 2017;7(18):4145-61.